



# ECSMGE 24

Lisbon, Portugal

## Geotechnical Engineering Challenges to Meet Current and Emerging Needs of Society

*Les Défis de la Géotechnique pour  
Répondre aux Besoins Actuels et  
Émergents de la Société*

Proceedings of the  
XVIII European Conference on  
Soil Mechanics and Geotechnical Engineering

*Comptes Rendus du  
XVIIIème Congrès Européen de  
Mécanique des Sols et de la Géotechnique*

Lisbon, 26-30 August 2024

**Editors**

Nuno Guerra, Manuel Matos Fernandes, Cristiana Ferreira, António Gomes Correia, Alexandre Pinto, Pedro Sêco e Pinto



[www.ecsmge-2024.com](http://www.ecsmge-2024.com)

## GEOTECHNICAL ENGINEERING CHALLENGES TO MEET CURRENT AND EMERGING NEEDS OF SOCIETY

‘Geotechnical Engineering Challenges to Meet Current and Emerging Needs of Society’ includes the papers presented at the XVIII European Conference on Soil Mechanics and Geotechnical Engineering (Lisbon, Portugal, August 26 to 30th, 2024). The papers aim to contribute to a better understanding of problems and solutions of geotechnical nature, as well as to a more adequate management of natural resources. Case studies are included to better disseminate the success and failure of Geotechnical Engineering practice. The peer-reviewed articles of these proceedings address the six main topics:

- New developments on structural design
- Geohazards
- Risk analysis and safety evaluation
- Current and new construction methods
- Environment, water, and energy
- Future city world vision

With contributions from academic researchers and industry practitioners from Europe and abroad, this collection of conference articles features an interesting and wide-ranging combination of innovation, emerging technologies and case histories, and will be of interest to academics and professionals in Soil Mechanics and Geotechnical Engineering.

PROCEEDINGS OF THE XVIII EUROPEAN CONFERENCE ON SOIL MECHANICS AND GEOTECHNICAL ENGINEERING, 26–30 AUGUST 2024, LISBON, PORTUGAL

COMPTES RENDUS DU XVIIIÈME CONGRÈS EUROPÉEN DE MÉCANIQUE DES SOLS ET DE LA GÉO-TECHNIQUE, 26-30 AOÛT 2024, LISBONNE, PORTUGAL

# Geotechnical Engineering Challenges to Meet Current and Emerging Needs of Society

*Les Défis de la Géotechnique pour Répondre aux Besoins Actuels et Émergents de la Société*

*Edited by*

Nuno Guerra

*NOVA University of Lisbon, Portugal*

Manuel Matos Fernandes

*University of Porto, Portugal*

Cristiana Ferreira

*University of Porto, Portugal*

António Gomes Correia

*University of Minho, Portugal*

Alexandre Pinto

*President of the Portuguese Geotechnical Society, Portugal*

Pedro Sêco e Pinto

*President of the Scientific Committee of ECSMGE 2024*



**CRC Press**

Taylor & Francis Group  
Boca Raton London New York Leiden

CRC Press is an imprint of the  
Taylor & Francis Group, an **informa** business

A BALKEMA BOOK

*Designed cover: Maria Brito and Leading*

First published 2025  
by CRC Press/Balkema  
4 Park Square, Milton Park, Abingdon, Oxon, OX14 4RN  
and by CRC Press/Balkema  
2385 NW Executive Center Drive, Suite 320, Boca Raton FL 33431

*CRC Press/Balkema is an imprint of the Taylor & Francis Group, an informa business*

© 2025 selection and editorial matter, Nuno Guerra, Manuel Matos Fernandes, Cristiana Ferreira, António Gomes Correia, Alexandre Pinto and Pedro Sêco e Pinto; individual chapters, the contributors

*Typeset by Integra Software Services Pvt. Ltd., Pondicherry, India*

The right of Nuno Guerra, Manuel Matos Fernandes, Cristiana Ferreira, António Gomes Correia, Alexandre Pinto and Pedro Sêco e Pinto to be identified as the authors of the editorial material, and of the authors for their individual chapters, has been asserted in accordance with sections 77 and 78 of the Copyright, Designs and Patents Act 1988.

The Open Access version of this book, available at [www.taylorfrancis.com](http://www.taylorfrancis.com), has been made available under a Creative Commons Attribution-Non Commercial-No Derivatives (CC-BY-NC-ND) 4.0 license.

Although all care is taken to ensure integrity and the quality of this publication and the information herein, no responsibility is assumed by the publishers nor the author for any damage to the property or persons as a result of operation or use of this publication and/or the information contained herein.

*British Library Cataloguing-in-Publication Data*

A catalogue record for this book is available from the British Library

*Library of Congress Cataloging-in-Publication Data*

A catalog record has been requested for this book

ISBN: 978-1-032-54816-6 (hbk)

ISBN: 978-1-003-43174-9 (ebk)

DOI: 10.1201/9781003431749

## Contents

Preface	xliv
Acknowledgements	xlvii
Editor Biographies	xlix
Advisory Committee <i>Comité Consultatif</i>	li
Scientific Committee <i>Comité Scientifique</i>	liii
Organizing Committee <i>Comité d'Organization</i>	lv
Board of Reviewers <i>Comité de Révision</i>	lvii

### **KEYNOTE LECTURES**

#### ***Conférences Principales***

On the interdependency between geotechnical and structural design <i>M. Topolnicki</i>	3
Geotechnical aspects of February 6, 2023 Kahramanmaraş-Türkiye earthquake sequence <i>K.O. Cetin, E. Cakir, A. Elsaid, F. Cuceoglu, B. Soylemez, S. Ocak &amp; B.U. Ayhan</i>	25
Risk analysis and mitigation in geotechnical engineering – Lessons learned from the collapse of the historical archive in Cologne due to underground construction <i>C. Moormann &amp; M.J.P. Effenberger</i>	45
How AI and IoT are transforming geotechnical site monitoring and construction <i>A. Gomes Correia &amp; E. Gastine</i>	72
Soil reinforcement based on bio-geo-chemical processes: from laboratory insights to field applications <i>L. Laloui, D. Terzis, R. Harran, J. Bosch, A. Elmaloglou, S. ten Bosch, M. Buyuklu &amp; Z.N. Sahlab</i>	84
3D planning in the Lisbon of the future: requirement or necessity? <i>C. Pinto</i>	96

### **STATE-OF-THE-ART REPORTS**

#### ***Rapports sur l'état de l'art***

Recent trends in monitoring tunnelling-induced displacements of structures <i>E. Bilotta</i>	113
High-speed rail earthworks design developments and innovative trials – building Britain's technical legacy <i>G. Katsigiannis</i>	127

Design and construction carbon reductions for HS2 station road network rail overbridge with polymer geogrid reinforced soil wall abutments and wingwalls on shallow foundations <i>C. Doulala-Rigby, M. Dalwadi, J. Belton, M. Duffy-Turner, R. Blackmore, G. Katsigiannis &amp; H.M.B. Al-Hashemi</i>	2895
A laboratory study of freeze-thaw effects on hydraulic conductivity of kaolin-sand mixtures <i>S. Feng, E. Ibraim &amp; P.J. Vardanega</i>	2901
Sustainable erosion control in geotechnical structures – case study <i>A. Ferreira, J. Sousa, J. Dias &amp; A. Neves</i>	2905
Enhancement of soil mechanical properties with biopolymers <i>N. Fradj, I. Kádár, K. Kopecskó &amp; A. Németh</i>	2909
Experimental study on the elasticity modulus of RCA-RTW mixtures <i>K. Gabryś &amp; W. Sas</i>	2915
The impact of geotechnical spatial variability on the installation of suction caisson anchors <i>E. Gallagher, S. Buykx, C. Reale &amp; D. Igoe</i>	2921
Insight into modelling offshore monopiles via 3D finite element analyses <i>D. Gaudio, A.B. Batilas, L.M. Lapastoure, A. Loukas, J. Lee, T. Joseph &amp; I. Thusyanthan</i>	2925
Technical solutions for reducing CO <sub>2</sub> footprint in MSE wall constructions <i>A. Grandclerc &amp; T. Joussellin</i>	2931
Why natural log of soil permeability is a linear function of void ratio for 0-400µm soils having a sandy-silty-clayey matrix? <i>J.C. Gress, M. Ferreira &amp; J.M. Cuinet</i>	2935
Theoretical assessment of the advective-diffusive transport of contaminants through landfill composite liners <i>N. Guarena, A. Dominijanni &amp; M. Manassero</i>	2939
The effect of soil type on the temperature-dependent strength parameters <i>M. Guner, S. Polat, U.C. Erginag, O. Cinicioglu, M. Sutman &amp; A. Hashemi</i>	2945
Preliminary study of the influence of marble dust on clayey soils improvement depending on the characteristics of the natural soil <i>E. Gutierrez, J.L. Pastor, M. Cano, A. Santos &amp; T. Hino</i>	2950
The use of LCA in a slope stability study for a quay rehabilitation assessment <i>E. Hafstad, G. Waldheim, A.B. Lundberg &amp; S. Larsson</i>	2955
Large-scale soil bio-cementation: insights into homogeneity, quality control, and waste handling <i>R. Harran, D. Terzis, M. Büyüklü &amp; L. Laloui</i>	2960
Thermal soil properties as a basis for design of underground high voltage cables <i>K. Hendler, C. Meier, S. Kleiber, J. Stegner, C. Drefke &amp; C. Boley</i>	2964
Validation of the applicability of the PS logger borehole probe for diverse geotechnical scenarios <i>R.M. Hen-Jones, P. Worthington, G. Comber, S. Garantini &amp; P.J. Vardanega</i>	2970
Impact of soil parameters on cyclic pull-out capacity of offshore screw anchors <i>C.F. Ho, A.P. Dyson &amp; A. Tolooiyan</i>	2974
Improving soil dry compaction by adding granular material <i>Y. Hocini, A. Medjnoun &amp; R. Bahar</i>	2978
Moisture content distribution in a dike cross-section – A case study of a geophysical investigation <i>Zs. Illés, G. Nagy, L. Nagy &amp; A. Kovács</i>	2982

# Insight into modelling offshore monopiles via 3D finite element analyses

## Considérations pour la modélisation de monopieux par élément finis 3D

D. Gaudio\*

*Dipartimento di Ingegneria Strutturale e Geotecnica, Sapienza Università di Roma, Rome, Italy*

A.B. Batilas, L.M. Lapastoure, A. Loukas, J. Lee, T. Joseph, I. Thusyanthan  
*Gavin & Doherty Geosolutions, Dublin, UK*

\*domenico.gaudio@uniroma1.it

**ABSTRACT:** Offshore wind farms have been attracting the attention of both researchers and practitioners over the past few decades, due to the growing interest in renewable energy. The choice of a particular foundation, which depends on several factors such as the mechanical properties of soil, depth to bedrock and bathymetry, may influence the overall wind farm cost by up to about 20%. Monopiles are the most used foundation system in the market, whose design can be further refined with advanced numerical analyses, provided that input parameters are properly calibrated. This paper shows the main results of a nonlinear static analysis of a monopile subjected to a horizontal load and embedded in a layered deposit. The analysis was performed using a 3D Finite Element model, where the foundation was represented with *plate* elements, and the soil mechanical behaviour was described with advanced constitutive models. The obtained pushover curves are shown and discussed, from which a reference design condition was selected. Then, the bending moment profile was obtained following three approaches, listed in a descending order of complexity: (1) integration of the stresses at the soil-*plate* interface; (2) derivation of the monopile rotation profile of the *plate* elements; (3) direct output from a *dummy beam* element located at the centreline of the monopile. It is shown that the *dummy beam* provides results in good agreement with those from the other two approaches, suggesting that it may be successfully adopted in practice to speed up the post-processing in the design of monopiles. The methodology presented in this paper would be useful for industrial projects.

**RÉSUMÉ:** Le développement des parcs éoliens en mer s'est accéléré au cours des dernières décennies grâce aux politiques publiques en matière d'environnement. Les monopieux sont le type de fondation le plus courant. Leur optimisation nécessite des modèles numériques avancés. Cet article présente les principaux résultats de la modélisation par éléments finis 3D d'un monopieu soumis à une charge horizontale. Dans cet exemple, le monopieux est installé dans un sol stratifié composé d'argile et de sable. Les résultats sont présentés en termes de déplacement et rotation du pieu sous l'effet du chargement latéral. L'évolution du moment de flexion le long du pieu est extrait de trois manières différentes: (1) par intégration des efforts à l'interface sol-pieu; (2) par dérivation du profil de rotation calculé à partir du déplacement des éléments coques qui modélisent le pieu; (3) à l'aide d'une poutre fictive modélisée au centre du pieu et qui permet de faciliter l'extraction des résultats. Cet exemple montre que les trois approches mènent à des résultats équivalents. Cela suggère que l'utilisation d'une poutre fictive peut être adoptée afin de faciliter et accélérer la modélisation des monopieux.

**Keywords:** Offshore wind turbines; monopiles; pushover analysis; 3D Finite Element model; *dummy beam*.

## 1 INTRODUCTION

Wind energy has emerged as a promising alternative energy source over the last few decades, to fill the world's energy supply and overcome some of the key issues associated with traditional fossil fuels, such as global warming. Particularly in Europe, offshore wind energy shows immense potential thanks to the presence of substantial portions of sea that are ideally suited for the construction of offshore wind farms (OWFs). Thanks to advancements in technology, OWFs have become profitable enough, despite their high construction costs, which depend not only on

governmental subsidies, but also on private support. Most of the OWFs budget is allocated to foundation design, construction, and installation. Despite other solutions being under development, monopiles are still the most used type of substructure.

In this paper, the main preliminary results of a nonlinear static (*i.e.*, pushover) analysis of a monopile embedded in a layered deposit are presented. The analyses were carried out with the Finite Element (FE) code *Plaxis 3D* (Bentley, 2023a), considering advanced constitutive models, capable of capturing the nonlinear and irreversible behaviour of the soil. The

results of the analyses are first given in terms of force-displacement and force-rotation curves, together with the bending moment profile developed in the monopile. The latter was computed following three approaches, namely: (1) integration of the stresses at the soil-plate interface; (2) derivation of the rotation profile obtained from the *plate* elements representing the monopile; (3) extraction of direct output from a *dummy beam* element located at the centreline of the monopile. It is shown that the *dummy beam* provides results in good agreement with the other two strategies, which may suggest adopting it in the practice to speed up the post-processing step in the design of monopiles.

## 2 PROBLEM DEFINITION

Figure 1 shows the soil profile considered in the study, together with the geometry of the monopile. The soil profile is composed of two units, namely a clayey and a sandy layer. The layer thickness is equal to 5.2 m for the clay layer and 9.3 m for the sand layer. The water table is located 0.6 m below ground level.

The monopile is a hollow steel pile with an outer diameter  $D = 2.0$  m, a wall thickness  $t = 0.035$  m, a length  $L = 11$  m ( $L/D = 5.5$ ), and an embedment depth  $H = 10.0$  m. Although the above dimensions are slightly smaller than those typically adopted for monopiles, they were considered in the numerical study for ease of numerical runs.

## 3 3D FINITE ELEMENT MODELLING

The Finite Element Analysis (FEA) was performed using the *Plaxis 3D* software to simulate the monotonic test under undrained conditions with a horizontal load applied atop the monopile, with a level arm  $e = 0.5$  m with reference to the ground surface.

The mechanical clay behaviour was modelled using the *NGI-ADP* constitutive model (Grimstad *et al.*, 2012), while the sand was simulated using the *HSS-small* (*HSS*) model (Benz *et al.*, 2009). The *NGI-ADP* constitutive model has been tailored to model the undrained behaviour of clays, matching both the undrained shear strength and strains at failure for three different stress paths *i.e.*, Active ( $s_u^A$ ), Direct Simple Shear ( $s_u^{DSS}$ ), and Passive ( $s_u^P$ ). The *HSS* model is simple to calibrate and yet capable of capturing the key soil behaviour for the problem under consideration, such as a good representation of the stiffness at small strains and the non-linear stiffness behaviour with increasing strain.

The monopile was modelled using linear elastic, homogeneous and isotropic 6-node triangular *plate* elements with five degrees of freedom per node and

quadratic shape functions, characterised by a wall thickness 0.035 m, a unit weight  $\gamma = 78.5$  kN/m<sup>3</sup>, a Young's modulus  $E = 199.2$  GPa, and a Poisson's ratio  $\nu = 0.3$ . The modulus is slightly lower than that of steel, as a consequence of the code interpreting the input diameter as a centreline diameter: hence, the Young's modulus was corrected so that the bending stiffness  $EI$  remained unaffected.

The behaviour of the interface within the soil-monopile zone was modelled with linearly elastic-perfectly plastic *interface* elements, whose coefficient of reduction of the shear strength was equal to  $R_{inter} = 0.7$  along the shaft and to  $R_{inter} = 1.0$  at the base. The FE model consisted of 18117 elements, extending by 40 m along the  $y$ -axis and by 16 m along the  $x$ -axis (Figure 2), corresponding to  $20 \cdot D$  and  $16 \cdot D/2$ , while the depth of the model was equal to 14.5 m. These model dimensions resulted from a preliminary sensitivity analysis, which showed that the boundaries did not affect the results when horizontal loads are applied atop the monopile. Also, they are in agreement with previous analyses performed on caisson foundations and onshore wind turbines under seismic loading (Gaudio *et al.*, 2016; 2023).

In the analysis, the monopile was applied a horizontal force at the top, along the  $y$ -direction: therefore, half of the domain was only modelled, due to the symmetry of the problem.

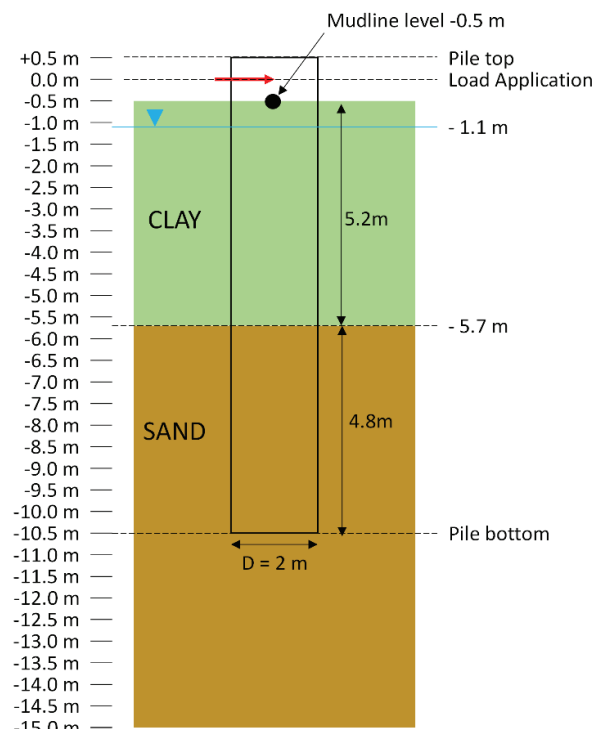


Figure 1. Soil profile and monopile geometry.



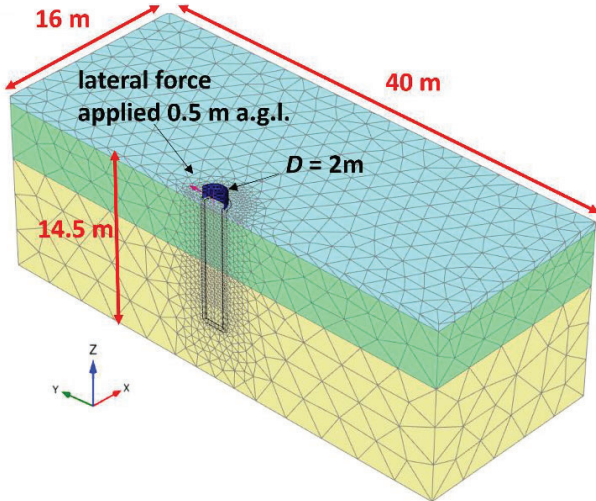


Figure 2. 3D Finite Element model adopted in the study.

### 3.1 Constitutive model soil parameters

The soil parameters of the constitutive models adopted in the FE analysis are listed in Table 1 and 2 for the *NGI-ADP* and the *HSS* models, respectively, which are representative of the mechanical behaviour of the clayey and sandy layers.

 Table 1. *NGI-ADP* parameters for the clay layer.

Soil parameter	Value	Units
$\gamma_{\text{sat}}$	17	[kN/m <sup>3</sup> ]
$\gamma'$	7	[kN/m <sup>3</sup> ]
$G_0/s_u^A$	500	[-]
$s_{u,\text{ref}}^A$	60	[kPa]
$s_{u,\text{inc}}^A$	0	[kPa/m]
$s_u^p/s_u^A$	0.50	[-]
$s_u^{\text{DSS}}/s_u^A$	0.75	[-]
$\gamma_f^C$	12	[%]
$\gamma_f^E$	24	[%]
$\gamma_f^{\text{DSS}}$	18	[%]
$\tau_0/s_u^A$	0	[-]
$k_0$	1	[-]

 Table 2. *HS-small* parameters for sand layer.

Soil parameter	Value	Units
$\gamma_{\text{sat}}$	18	[kN/m <sup>3</sup> ]
$\gamma'$	8	[kN/m <sup>3</sup> ]
$E_{50}^{\text{ref}}$	69.6	[MPa]
$E_{\text{Oed}}^{\text{ref}}$	69.6	[MPa]
$E_{\text{ur}}^{\text{ref}}$	208.7	[MPa]
$G_0^{\text{ref}}$	200	[MPa]
$\nu^{\text{ur}}$	0.25	[-]
$m$	0.5	[-]
$\gamma_{0.7}$	0.015	[%]
$\phi'$	40.0	[°]
$\phi'_{\text{cv}}$	32.0	[°]
$\psi$	9.9	[°]
$k_0$	0.357	[-]
<i>OCR</i>	6	[-]

## 4 PUSHOVER CURVES

The results obtained from the nonlinear static analysis are discussed in this paragraph, which was performed as a *Plastic* calculation in Plaxis 3D. The monotonic response of the monopile is presented in Figure 3 in terms of the lateral load against the horizontal pile displacement and rotation of the monopile at the mudline level (see Figure 1).

As expected, the non-linear behaviour of the soil-monopile system was triggered from low levels of horizontal displacement. The displacement  $y = D/10 = 0.20$  m is also marked in Figure 3, which was taken as a reference design condition for the assessment of the bending moment acting into the monopile, to compare against the yield moment,  $M_y$ , as discussed in the following section. The horizontal load  $H_{0.1D} = 3076$  kN was computed for this design condition, which corresponded to a rotation  $\theta = 1.49^\circ$ .

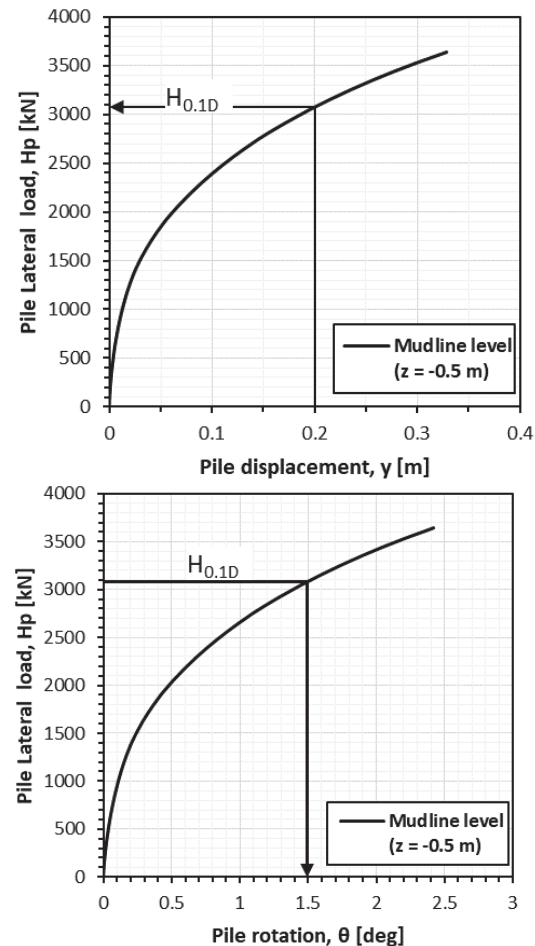


Figure 3. Monotonic pile response at the mudline level.

## 5 BENDING MOMENT PROFILES

The structural checks of the foundation were made by comparing the maximum bending moment

experienced by the monopile for the reference design condition mentioned above. To this end, the bending moment profile was first evaluated, following three different approaches, such as: (1) integration of the stresses at the soil-plate interface; (2) derivation of the rotation profile of the plate elements simulating the monopile; and (3) extraction of a direct output from the dummy beam element located at the centreline of the monopile.

The results obtained with the three approaches are compared in the next sections, after introducing them in a descending order of complexity.

### 5.1 Stress integration at the soil-plate interface

The bending moment profile was first calculated from the integration of stresses acting at the soil-plate interface as below:

$$M_{i,s} = H_p \times e + \int_0^{z_i} [p(z) \times \Delta z] \cdot dz + \int_0^{z_i} m(z) \cdot dz \quad (1)$$

where subscript  $i$  represents a depth counter ( $i = 1 \text{ m}, 0.5 \text{ m}, 0, \dots, -10.5 \text{ m}$ ),  $H_p$  is the lateral force applied atop the monopile,  $e = 0.5 \text{ m}$  is the distance between the lateral load and the mudline level,  $p(z)$  and  $m(z)$  are the distributed lateral reaction and moment applied by the soil to the monopile, respectively, and  $\Delta z = 0.5 \text{ m}$  is the depth interval selected for integration (Figure 4). The distributed lateral reaction  $p(z)$  was computed from the integration of the interface forces along the  $y$ -direction, while the distributed moment,  $m(z)$ , was obtained from the integration of forces along the  $z$ -direction, multiplied by the respective lever arm  $y = D/2 = 1 \text{ m}$ :

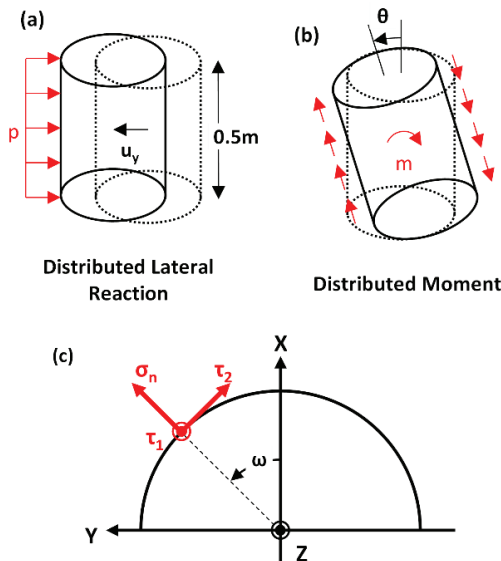


Figure 4. Distributed (a) lateral load  $p(z)$  and (b) moment  $m(z)$ ; (c) local coordinate system.

$$p(z) = \frac{\int_{z-\Delta z/2}^{z+\Delta z/2} F_y(z) \cdot dz}{\Delta z} \quad (2)$$

$$m(z) = \frac{\int_{z-\Delta z/2}^{z+\Delta z/2} F_z(z) \times y \cdot dz}{\Delta z} \quad (3)$$

where  $F_y$  and  $F_z$  are the forces along the  $y$  and  $z$ -direction, respectively.

Only stresses in local coordinates are accessible rather than forces  $F_y$  and  $F_z$  in the FE analysis, where  $\sigma_n$  is the stress normal to the interface, while  $\tau_1$  and  $\tau_2$  are the vertical and horizontal tangential stresses, respectively (Figure 4). The stresses were translated into forces as in eqs. (4) and (5) below, for every stress point, *i.e.*, for a given pair of coordinates,  $x$  and  $y$ , element area,  $A$ , and integration weight,  $w$  (Bentley, 2023b):

$$F_y(z) = w \cdot A \cdot [\sigma_n(z) \sin \omega - \tau_2(z) \cos \omega] \quad (4)$$

$$F_z(z) = w \cdot A \cdot \tau_1(z) \quad (5)$$

### 5.2 Derivative of rotations of plate elements

The bending moment profile was also calculated from the plate elements representing the monopile. To this end, the steps reported below were followed, starting from the vertical displacement of the two ends of the plates, whose sign convention is depicted in Figure 5:

- extraction of the back and front vertical displacement of the plate,  $u_{z,i}^{\text{front}}$  and  $u_{z,i}^{\text{back}}$ , respectively;
- calculation of the pile rotation,  $\theta_i$ , at the  $i^{\text{th}}$  depth ( $i = 1 \text{ m}, 0.5 \text{ m}, 0, \dots, -10.5 \text{ m}$ ) as:

$$\theta_i = \tan^{-1} \left( \frac{u_{z,i}^{\text{back}} - u_{z,i}^{\text{front}}}{D} \right) \quad (6)$$

- computation of the bending moment at the  $i^{\text{th}}$  depth ( $i = 1 \text{ m}, 0.5 \text{ m}, 0, \dots, -10.5 \text{ m}$ ),  $M_{i,p}$ , from the derivative of the pile rotation with depth (*i.e.*, curvature), where  $EI$  represents the bending stiffness of the monopile ( $E = \text{Young's modulus}$ ,  $I = \text{moment of inertia around the vertical axis}$ ) as:

$$M_{i,p} = EI \cdot \frac{d \tan \theta_i}{dz} = EI \cdot \left( \frac{\theta_i - \theta_{i+1}}{z_i - z_{i+1}} \right) \quad (7)$$

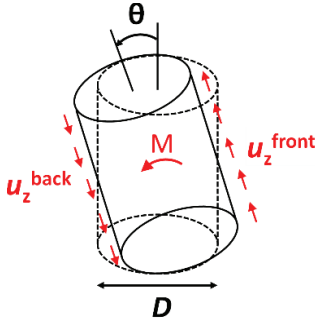


Figure 5. Calculation of the bending moment from plate elements.

### 5.3 Direct output from the dummy beam

Finally, the bending moment profile of the monopile was also obtained from a *dummy beam*, which was introduced at the centreline of the monopile. It is worth noting that this approach has already been routinely followed for excavation wall simulations in 2D conditions, when using continuum elements to model the wall and postprocessing the wall bending moments (Lam, 2018).

The stiffness of the *dummy beam* was selected to be low (*i.e.*,  $E_{\text{real}}/E_{\text{dummy}} \approx 1000$ ) in order to not affect the results, as this beam was only used as a trick to avoid either integrating stresses acting along the shaft of the monopile or differentiating the *plate* rotation profile. Therefore, a Young's modulus  $E_{\text{dummy}} = 210$  MPa was assigned to the *dummy beam* element, since the “real” Young's modulus of the monopile was the one of steel,  $E_{\text{real}} = 199.2$  GPa (see § 3). As for the moment of inertia of the dummy beam, only half of the monopile inertia was considered thanks to the symmetry of the problem, *i.e.*, for the original diameter  $D = 2$  m, the moment of inertia of the *dummy beam* was  $I = 1/2 \cdot \pi/64 \cdot [D^4 - (D - 2t)^4] = 0.05216$  m<sup>4</sup>. The bending moment profile was then extracted as follows:

$$M_{i,b} = \frac{(EI)_{\text{real}}}{(EI)_{\text{dummy}}} \times M_{\text{dummy},i} = 1897 \times M_{\text{dummy},i} \quad (8)$$

### 5.4 Comparison of bending moments profiles

A comparison of the bending moment profiles obtained with the three strategies above is made in Figure 6. The bending moments were computed for the design at the reference condition of a horizontal displacement  $y = D/10 = 0.20$  m at mudline level. In the figure, the bending moment at yield,  $M_y = 33.9$  MN·m, is also plotted.

From Figure 6 it is evident that the three solutions provide quite similar results, both in terms of the bending moment profile and its maximum value. In

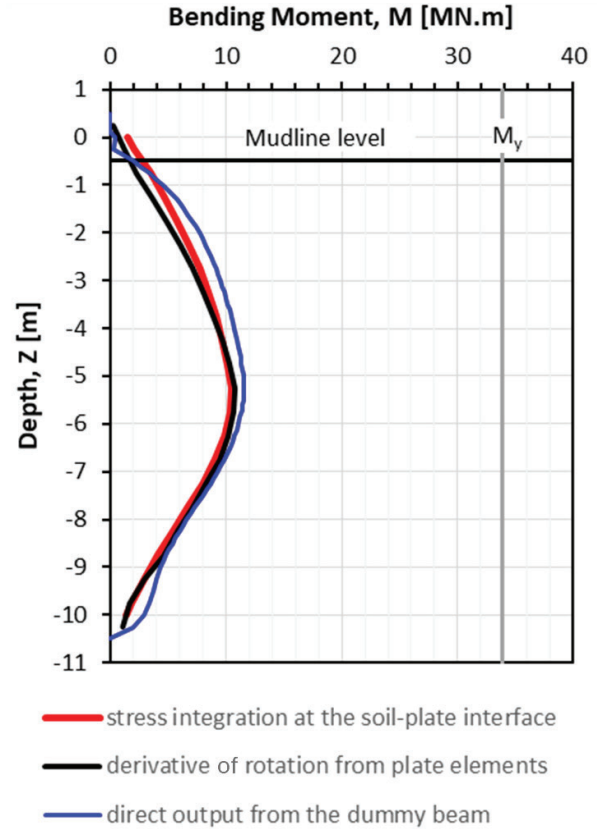


Figure 6. Bending moment profiles along the monopile computed with the three approaches adopted in the study.

particular, it is shown that the maximum bending moment from the stress integration (red line) was equal to  $M_{\text{max},s} = 10.4$  MN·m, while the one from the derivative of the monopile rotation (black) was equal to  $M_{\text{max},p} = 10.8$  MN·m, with negligible deviation of about 4.0%. As for the profile from the *dummy beam* (blue), the peak bending moment is equal to about  $M_{\text{max},b} = 11.5$  MN·m, which corresponded to an overestimation of 1.1 MN·m (~ 9.6%) and 0.7 MN·m (~ 6.1%) from the maximum values obtained from the stress integration and the derivative of rotations from the plate elements, respectively. This result shows that the *dummy beam* provides results in a good agreement with the other two strategies, which may suggest adopting it in the practice in the design of monopiles. Based on project experience of the Authors, the best method to derive the bending moment profile was the derivative of rotation from *plate* element method. The results above are summarised in Table 3.

Table 3. Summary of maximum bending moments (MN·m).

Approach	Value [MN·m]	Comparison with the dummy beam
stress integration	10.4	- 9.6%
rotation derivative	10.8	- 6.1%
<i>dummy beam</i>	11.5	/

## 6 CONCLUSIONS

The market of offshore wind turbines has been expanding over the last decades due to climate change, thereby increasing focus on the design of the foundation system, which can represent up to about 20% of the cost of the entire wind farm. Innovative solutions and design methods have therefore been sought to reduce costs of the foundation system.

In this paper, the results of a 3D Finite Element pushover analysis conducted on a monopile embedded in a layered deposit have been presented. In the analyses, the monopile was simulated through *plate* elements and subject to a horizontal force applied to the top of the foundation. The resulting force-displacement and force-rotation pushover curves have been first shown and discussed to detect a reference design condition for the monopile, corresponding to a horizontal displacement at the mudline level equal to one tenth of the outer diameter.

Then, the bending moment profile developed in the monopile has been computed. For the design condition, three different approaches have been used to determine this profile which include the integration of the stresses at the soil-*plate* interface, the derivation of the rotation profile obtained from the *plate* elements representing the monopile, and the extraction of direct output from a *dummy beam* located at the centreline of the monopile. It has been shown that the *dummy beam* provides results in good agreement with the other two strategies, which may suggest adopting it in the practice to speed up the post-processing step in the design of monopiles. It is worth noting that the Timoshenko's beam theory has been adopted in this study, which means that the beam deflection comes both from bending and shearing. This is expected to be well representative of the real behaviour for the monopile at hand. A discussion on the pitfalls of the deterministic approach followed for the *dummy beam* is given in Beck and Silva Jr. (2011).

The capability of 3D Finite Element models of capturing the main features of the soil-monopile behaviour under consideration would always involve a level of uncertainty. It is recommended that these models and results are validated using field-test results or case histories from existing literature.

## ACKNOWLEDGEMENTS

The first author is grateful for the financial support provided by Ministero dell'Università e della Ricerca

(Italy) through the project PON "Ricerca e Innovazione" 2014-2020.

## REFERENCES

- Beck, A. T., da Silva Jr, C. R. (2011). Timoshenko versus Euler beam theory: Pitfalls of a deterministic approach. *Structural Safety*, 33(1): 19-25, <https://doi.org/10.1016/j.strusafe.2010.04.006>.
- Bentley (2023a). *PLAXIS 3D 2023.1: General Information Manual 3D* (Available at: [https://communities.bentley.com/cfs-file/\\_key/communityserver-wikis-components-files/00-00-00-05-58/PLAXIS\\_5F00\\_3D\\_5F00\\_2023.1\\_5F00\\_3D\\_5F00\\_0\\_5F00\\_General-Information-Manual.pdf](https://communities.bentley.com/cfs-file/_key/communityserver-wikis-components-files/00-00-00-05-58/PLAXIS_5F00_3D_5F00_2023.1_5F00_3D_5F00_0_5F00_General-Information-Manual.pdf), accessed: 12/03/2024).
- Bentley (2023b). *PLAXIS 3D 2023.1: Scientific Manual 3D* (Available at: [https://communities.bentley.com/cfs-file/\\_key/communityserver-wikis-components-files/00-00-00-05-58/PLAXIS\\_5F00\\_3D\\_5F00\\_2023.1\\_5F00\\_3D\\_5F00\\_4\\_5F00\\_Scientific-Manual.pdf](https://communities.bentley.com/cfs-file/_key/communityserver-wikis-components-files/00-00-00-05-58/PLAXIS_5F00_3D_5F00_2023.1_5F00_3D_5F00_4_5F00_Scientific-Manual.pdf), accessed: 12/03/2024).
- Benz, T., Vermeer, P. A., Schwab, R. (2009). A small-strain overlay model. *International Journal for Numerical and Analytical Methods in Geomechanics*, 33(1): 25-44, <https://doi.org/10.1002/nag.701>.
- Gaudio, D., Rampello, S. (2016). Dynamic soil-structure interaction of bridge-pier caisson foundations. In *Geotechnical engineering in multidisciplinary research: from microscale to regional scale CNRIG2016. VI Italian Conf. of Researchers in Geotechnical Engineering, Procedia Engineering*, Elsevier, 158: 146-151, <https://doi.org/10.1016/j.proeng.2016.08.420>.
- Gaudio D., Seong J., Haigh S., Viggiani G. M. B., Madabhushi G. S. P., Shrivatsava R., Veluvolu R., Padhy P. (2023). Boundary effects on dynamic centrifuge modelling of onshore wind turbines on liquefiable soils. *International Journal of Physical Modelling in Geotechnics*, ICE Publishing, 23(1): 16-34, ISSN: 1346-213X, <https://doi.org/10.1680/jphmg.21.00085>.
- Grimstad, G., Andresen, L., Jostad, H. P. (2012). NGI-ADP: Anisotropic shear strength model for clay. *International Journal for Numerical and Analytical Methods in Geomechanics*, 36(4): 483-497, <https://doi.org/10.1002/nag.1016>.
- Lam, A. K. (2018). An engineering solution for a hillside project in Hong Kong. *Geotechnical Research*, ICE Publishing, 5(3), 170-181, <https://doi.org/10.1680/jgere.18.00008>.